Received: 24 June 2022 | Revised: 31 October 2022 | Accepted: 20 November 2022

IET Electrical Systems in Transportation

DOI: 10.1049/els2.12063

The Institution of Engineering and Technology WILEY

ORIGINAL RESEARCH

Performance analysis of dual stator six-phase embedded-pole permanent magnet synchronous motor for electric vehicle application

Raja Ram Kumar[1] | Priyanka Devi[2] | Chandan Chetri[2] | Ankita Kumari[2] | Papu Moni Saikia[2] | Ram Khelawan Saket[3] | Kundan Kumar[4] | Baseem Khan[5]

[1]Department of Electrical Engineering, Ghani Khan Choudhury Institute of Engineering & Technology, Malda, West Bengal, India

[2]Department of Electrical Engineering, Jorhat Engineering College, Jorhat, Assam, India

[3]Department of Electrical Engineering, India Institute of Technology (BHU), Varanasi, Uttar Pradesh, India

[4]Department of Electrical Engineering, National Institute of Technology, Imphal, Manipur, India

[5]Department of Electrical and Computer Engineering, Hawassa University, Hawassa, Ethiopia

Correspondence

Baseem Khan, Department of Electrical and Computer Engineering, Hawassa University, Hawassa, Ethiopia.
Email: baseem.khan04@gmail.com

Funding information

Science and Engineering Research Board; Department of Science & Technology; Government of India, Grant/Award Number: EEQ/2021/000177

Abstract

The motive of this study is to analyse the characteristics of a novel dual-stator embedded-pole six-phase permanent magnet synchronous motor for the application of electric vehicles. A comparative analysis of two separate motor topologies, namely, dual stator embedded-pole six-phase permanent magnet synchronous motor and single stator single rotor surface-mounted permanent magnet synchronous motor, is accomplished to illustrate the performance superiority of the proposed motor. Furthermore, for optimal designing of the proposed motor, a design methodology has also been presented. For the above application, the motor should retain high torque density (HTD) and high reliability. In this regard, a novel H-Shaped flux barrier is introduced in the rotor portion, which fulfils the requirement of HTD. Moreover, the availability of two sets of the stator winding enhances the performance efficiency and ensures the proposed motor's more significant fault-tolerating ability of the motor. For performance evaluation, the Finite Element Method analysis is chosen, as it gives appropriate and precise results. From the above analysis, it is concluded that the HTD and the proposed motor's dynamic performance are better than the above-mentioned conventional motor.

KEYWORDS

dual stator, electric vehicle, embedded-pole, FEM, H-shaped flux barrier, multi-phase, PMSM

1 | INTRODUCTION

India is highly dependent on the import of crude oil. In the past decade, it has imported around 80% of total oil consumption [1]. The majority of this oil is used in the form of gasoline, diesel etc. in automobile applications only. Due to this high dependency on crude oil, the automotive industries are intended to adapt to the latest technologies which use alternative fuels. As a result, several manufacturing companies have started producing Electric or Hybrid-Electric Vehicles instead of Fuelled vehicles.

These Electric Vehicles are generally the only vehicles to adequately meet the growing demand for gasoline shortly [2–4]. These vehicles are fuelled with electricity, thus minimising the use of oils and emission of greenhouse gases, noise, and pollutants, compared to conventional vehicles [5–7]. Several

motors can be employed in Electric Vehicles such as Induction motors, Brushless DC motors (BLDC), Brushed DC motors, and permanent magnet synchronous motors (PMSM) [8–11]. Brushed DC motors are capable of producing high torque, but the brushes lead to wear and tear of the commutator, thereby limiting the overall motor rpm. In its comparison, DC brushless motors have higher performance and lower maintenance. Due to high performance and good speed control, three-phase induction motors are also commonly used in electric vehicles. But amongst them, the PMSMs are getting much more popular, as it does not wish for any external excitation to make the rotor in motion, unlike the other DC and induction motors. Also, it has a very high durability, compact construction and is capable of generating high power density too [12–16]. Other than these, the PMSM has advantages such as less maintenance cost, absence of additional noise, HTD etc. [17–19]. Owing to these benefits, some of the prominent car manufacturers such as Toyota, Nissan, Mitsubishi etc. are actively using PMSM to produce EVs [20]. In PMSM, the arrangement of magnets in the rotor has a vital role in boosting the overall efficiency of the system. It may be surface-mounted magnets, where the magnets are simply fixed at the rotor surface [21, 22] or embedded-pole, where the magnets are buried inside the rotor [23, 24]. The surface-mounted machines provide high power density and are more cost-effective than the embedded pole machines [25, 26]. But in terms of reliability, the embedded pole machines are much better than the surface-mounted ones. For high-speed applications, the embedded pole magnets are preferred, due to their magnet orientation [27, 28]. Moreover, it is pointed out that the concept of the embedded pole magnet has been utilised in many permanent magnet synchronous machines to enhance various performance parameters. In Ref. [29], tooth-coil winding PM synchronous machines (TCW PMSM) with embedded pole magnets are used up for torque ripple reduction. In Ref. [30], PM-switched reluctance motors (PM-SRM) with the embedded PM are utilised for torque enhancement. In Ref. [31], the problem of demagnetisation of PM for permanent magnet-assisted synchronous reluctance motor (PMa-SynRM) is highlighted. The concept of a multilayer flux barrier with an embedded pole is used for the design of PMa-SynRM to enhance features like reluctance torque and saliency. In Ref. [28], to resolve the asymmetrical issues in magnetically geared machines, the authors have proposed a novel structure called consequent pole magnetic geared machines (CP-MGM). The CP-MGM makes use of the axially embedded PM to obtain an enhanced torque and symmetrical BEMF. The comparison of mentioned embedded pole machines is depicted in Table 1. Nowadays, in PMSM, the dual stator system is getting more prominent rather than the single stator system [32]. That is because, in the dual stator configuration, the power flowing to the load from both the outer and inner stator terminals is summed up and thereby provides a high density for rotating the rotor [33]. In this study, the authors have proposed a novel dual stator embedded-pole six-phase PMSM (NDSEPSP-PMSM) with flux barriers for an electric vehicle application. Here, the rotor is present in between the two stators, and the magnets are embedded inside it. Moreover, the rotor is shaped uniquely. It is observed that the adjacent embedded magnets in the rotor are connected through a thin portion of the rotor, and the remaining portion of that rotor region is sliced off. Due to this, the flux barrier is named an H-Shaped flux barrier. It describes the uniqueness inculcated in the rotor, which reduces the flux leakage in it and thus proves the machine's novelty. For the improvement of TD and FTA, the six-phase winding is furnished in both stators. Also, the level of acoustic noise and ripple production is minimised remarkably in the case of six-phase machines as compared to the three-phase machines [34, 35]. Moreover, lower current rating semiconductor devices are required for the converter utilised in the six-phase PMSM as compared to the three-phase PMSM. Hence, due to the lower rating of devices, the size of the required heat sink will be minimised to a greater extent.

Further, it is found that researchers have established many research works, as shown in Table 2, which shows a comparative study of the proposed motor with the existing and conventional motors.

The motive behind this comparative study is to demonstrate the superior properties present in the proposed motors. For comparison, many parameters are taken into account, such as magnetic flux density, power rating, BEMF, torque, ripple torque etc. In Ref. [36], a comparative study between conventional series hybrid magnets Variable Flux Memory Machines (VFMM) and novel parallel hybrid magnets VFMM has been performed. The performance of the new VFMM parallel hybrid magnets has been improved to a larger extent (high-speed regions). The parameters utilised for the purpose of comparison are enlisted in Table 2. In Ref. [37], the authors have evaluated the electromagnetic performance of traction motors for EVs. For the purpose of comparison, different types of traction motors are

TABLE 1 Embedded pole machines

Embedded pole machines	[29]	[30]	[31]	[28]	Unit
Name of the machine	TCW PMSM	PM-SRMs	PMa-SynRM	CP-MGM	NDSEPSP-PMSM
Novelty on the basis of flux barrier	No novelty found	No novelty found	A multi-layer flux barrier is found which improves the torque but it has utilised a large amount of PM which makes the machine costlier.	No novelty found	An H-shaped flux barrier is found which enhances the torque density with a minimum utilisation of PM

TABLE 2 Parameter index considered for comparison of motors

Parameter index	[36]	[37]	[38]	[39]	[40]	Proposed motor
Flux density	√	√	√	√	√	√
Power rating	√	√	√	√	√	√
BEMF	√	√	√	√	√	√
% THD						√
Torque	√	√	√	√	√	√
% Ripple torque	√					√
Losses	√			√		√
Efficiency	√	√	√		√	√
Cogging torque					√	√
Torque density						√
Temperature distribution	√	√		√		

utilised, namely, permanent magnet-assisted synchronous reluctance motors and interior permanent magnet motors. The results of the study indicate the merits and demerits of these motors for traction application, and it provides some beneficial recommendations for the designing of traction motors. The parameters considered for comparison are enlisted in Table 2. In Ref. [38], in order to resolve the problems of the motor having rare-earth PMs, the authors have compared two motors, namely, a multi-layer interior permanent magnet and a concentrated flux synchronous motor, using ferrite PMs. It is found that each motor has several merits, including the lower cost (due to the utilisation of ferrite PM) as compared with rare-earth PM motors. The parameters considered for comparison are listed in Table 2. In Ref. [39], for high-speed applications, a comparison of interior permanent-magnet (IPM) motors and surface-mounted permanent-magnet (SPM) has been done. It is found that the IPM is a better choice with respect to cost while SPM is more reliable, with higher efficiency. The parameters considered for the comparative study are enlisted in Table 2. Similarly, in Ref. [40], a comparison of a five-phase outer-rotor flux-switching permanent magnet with four different configurations, namely, single-layer winding, double-layer winding, E-core, and C-core has been evaluated. The objective of this comparative analysis is to highlight the superiorities of the motors based on their performance characteristics. The parameters considered for comparison are enlisted in Table 2.

Following the present trend of a comparative study, the authors have compared the proposed NDSEPSP-PMSM with an H-shaped flux barrier, with two different topologies, namely, DSEPSP-PMSM without flux barrier and SSSRSM-PMSM. Here, the test is conducted based on the parameters taken in Table 2 for better comparison. For the design and analysis of these three models, the authors opted for the Finite Element Method (FEM), which gives accurate results [41, 42]. The Finite Element Method (FEM) is a computational procedure engaged to perform finite element analysis. It requires the domain to be estimated into a finite number of sections (or components) for simplicity [43]. Through FEM, magnetostatics and transient analysis of the model are done. For magnetostatics, a static magnetic field is required, and for the transient analysis, a transient magnetic field of PM is determined.

The following points mentioned below illustrate the major goal of this paper:

1. A NDSEPSP-PMSM with an H-shaped flux barrier is proposed for electric vehicle application.
2. To highlight the superior performance of the proposed NDSEPSP-PMSM (with flux barrier), a comparative study has been established with two different topologies, namely, DSEPSP-PMSM (without flux barrier) and SSSRSM-PMSM.

The paper has been framed as Section 2, which introduces the structure, specification, principal operation, and methodology of optimal design of the proposed motor. Section 3 covers the FEM analysis, and Section 4 focuses on optimal design and performance analysis. Finally, the paper concludes with Section 5.

2 | STRUCTURAL DESCRIPTION OF DIFFERENT TOPOLOGIES

The diagrams of NDSEPSP-PMSM with H-shaped flux barriers and two different topologies, namely, DSEPSP-PMSM (without flux barrier) and SSSRSM-PMSM are shown in Figure 1a,b,c, respectively. The NDSEPSP-PMSM and DSEPSP-PMSM have a single rotor, which is sandwiched with two stators (inner and outer), whereas the SSSRSM-PMSM includes a single stator and a single rotor.

The stators of all the topologies are housed with 60 slots, 10-pole, and a six-phase integral slot double layer winding arrangement. The outer stator is having 60 conductors/slot (with a coil span of six), whereas the inner stator is having 30 conductors/slot (with a coil span of six). The rotors have 10 embedded-pole of magnets. With respect to the suitable position of the novel H-shaped flux barriers, it is inferred that the local leakage of the flux in NDSEPSP-PMSM is reduced to a huge extent as compared with DSEPSP-PMSM. Simultaneously, the air gap flux density is also enhanced in the NDSEPSP-PMSM. This limited nature of a leakage flux along with increased air gap density defines the novelty of NDSEPSP-PMSM. Moreover, it is observed that due to the introduction of H-shaped flux berries, the mechanical strength of the rotor reduces to some extent. But, this can be compensated by means of a non-magnetic special rotor frame. Further, certain advantageous features like maximum utilisation of iron material, lightweight, and robustness are

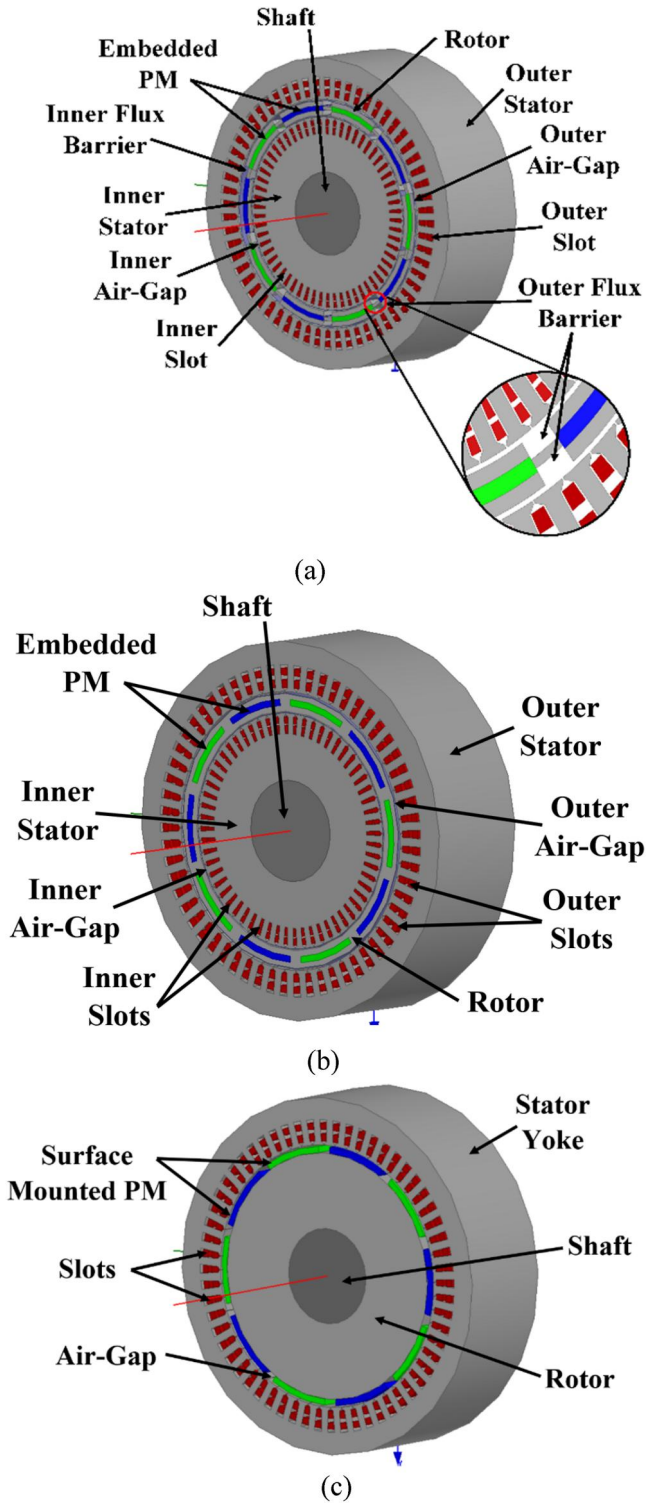

FIGURE 1 Schematic of the proposed topologies (a) novel dual-stator embedded-pole six-phase permanent magnet synchronous motor (with H-shaped flux barrier), (b) dual stator embedded-pole six-phase permanent magnet synchronous motor (without flux barrier), and (c) single stator single rotor surface-mounted permanent magnet synchronous motor

pointed out in NDSEPSP-PMSM. Also, the magnets in NDSESP-PMSM are embedded in the centre of the rotor, which results in equal air gap flux in the outer and inner air gaps. On the other hand, with the utilisation of the same volume of magnets, it is observed that due to dual stator configuration, the torque to weight ratio is higher in NDSEPSP-PMSM and DSEPSP-PMSM as compared with conventional single stator motors. The machine designing details of NDSEPSP-PMSM, DSEPSP-PMSM, and SSSRSM-PMSM are enlisted in Table 3.

TABLE 3 Dimensional Parameter (in mm) of PMSMs

Parameter	NDSEPSP-PMSM	DSEPSP-PMSM	SSSRSM-PMSM
Outer radius of outer stator	150	150	150
Inner radius of outer stator	110	110	110
Outer radius of inner stator	93	93	-
Inner radius of inner stator	40	40	-
Outer radius of rotor	108.5	108.5	103.5
Inner radius of rotor	94.5	94.5	40
Width of magnets	5	5	5
Air gap length	1.5	1.5	1.5
Radius of the shaft	40	40	40
No. of conductors in outer stator (conductors/slot)	60	60	60
No. of conductors in inner stator (conductors/slot)	30	30	-
Coil span for the outer stator winding	6	6	6
Coil span for the inner stator winding	6	6	-

2.1 | Principle of operation of electric vehicle

Figure 2a shows the operational diagram of the electric vehicle. There are five main components of an electric vehicle namely battery, converter, controller, PMSM, and gearbox system. The prime power source of electric vehicles is series and parallel combinations of batteries. It supplies power to a six-phase converter (DC to AC) and then through the controller, power is supplied to the AC motor. There are three motors presented in this study, with each of them having 10-poles on the rotor. When fluxes from both the rotor and stator interact, it produces a torque on the rotor. This power of the motor can be transmitted to the wheels through the gearbox. During regenerative braking, the power of the motor can be utilised for charging the batteries.

2.2 | Methodology of design

Figure 2b shows the methodology used to optimally design the proposed motor. At first, it is crucial to set various

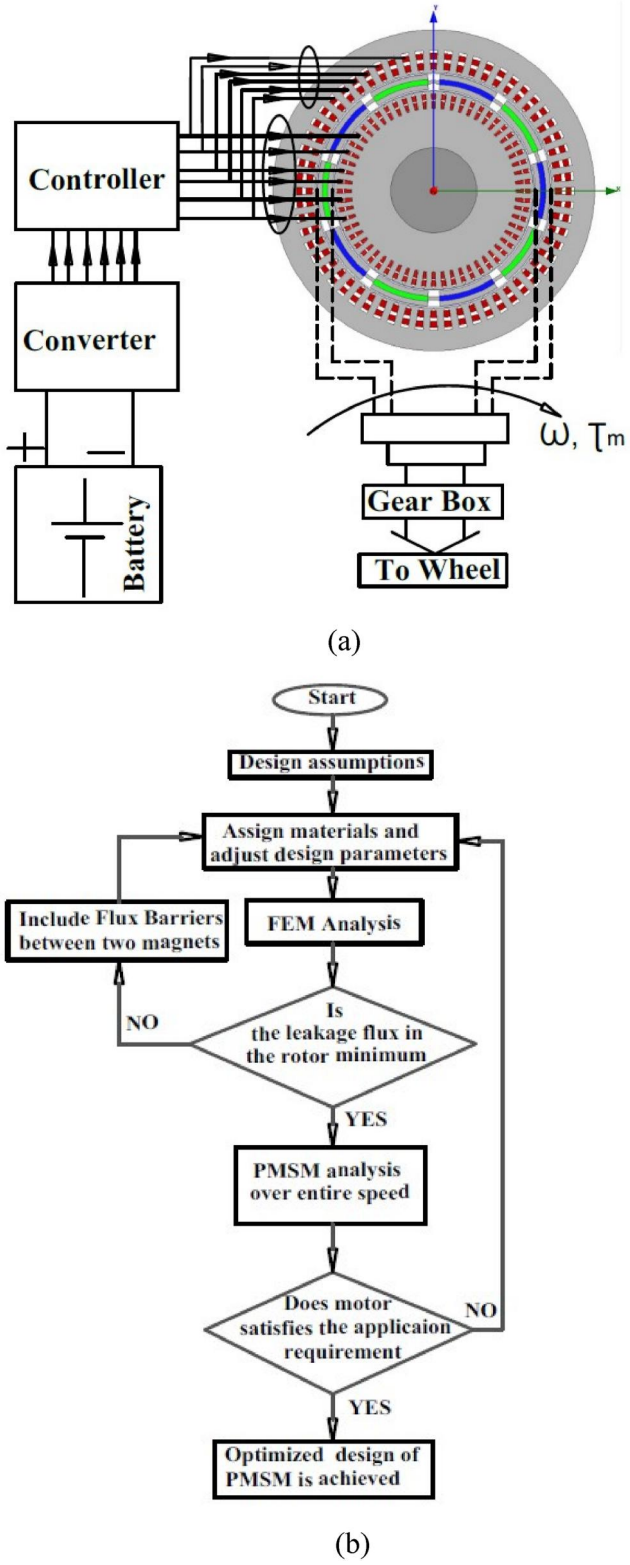

FIGURE 2 Permanent magnet synchronous motors (PMSM) drive- (a) EV operating Principal and (b) Design methodology of PMSM

design assumptions after which the adjustment of the design parameter and assigning material properties for different portions of the motor are done. After this, FEM analysis has been done to check whether the leakage flux in the rotor is minimum or not. If not, then it is required to include the flux barrier between two magnets and then again adjust the design parameters. If yes, then an analysis of the motor for a full range of speed and current has to be done. After that, it is required to check whether the motor performance is suitable for the application or not. If not, then again it needs to adjust the machine parameter and follow all the above steps. If yes, then the motor design is considered as the final optimal design of the motor.

3 | FINITE ELEMENT METHOD

The proposed NDSEPSP-PMSM (with flux barrier) and DSEPSP-PMSM (without flux barrier) include a dual stator and a single rotor. At the same time, SSSRSM-PMSM contains a single rotor and a single stator system. Further, for the optimal designing and analysis of the mentioned different topologies, the FEM is proved to be the best choice, as it provides precise results.

The steps to be followed for the FEM analysis are-

a. To create a model
b. To allocate material property
c. To assign boundary conditions
d. To assign rotatory rotor band (600 rpm)
e. To provide excitation
f. Perform meshing
g. Analysis set-up
h. Evaluating results

To evaluate the performance of different topologies (as mentioned in the paper), two methods of the solver are opted, namely magnetostatic and transient.

Elemental plots for various topologies, namely NDSEPSP-PMSM, DSEPSP-PMSM, and SSSRSM-PMSM are represented in Figure 3a,b,c, respectively. With proper selection of edge lengths of various topologies, the number of finite elements is observed to be as follows:

a. NDSEPSP-PMSM- 61,854.
b. DSEPSP-PMSM- 59,684.
c. SSSRSM-PMSM- 63,277

Figure 4a highlights the flux line distribution of a conventional DSEPSP-PMSM (without flux barrier), which has 10 magnetic poles inside the rotor. From the diagram, it is noticed that there is a high density of flux lines towards the ends of two adjacent magnets. This is due to a local (magnet to adjacent magnet and magnet to the same magnet via iron) leakage of flux, which occurs due to the flux getting interlinked from one magnet to the other from the path inside the rotor. This phenomenon of the local leakage flux decreases the average density of the air gap flux in DSEPSP-PMSM. Moreover, to

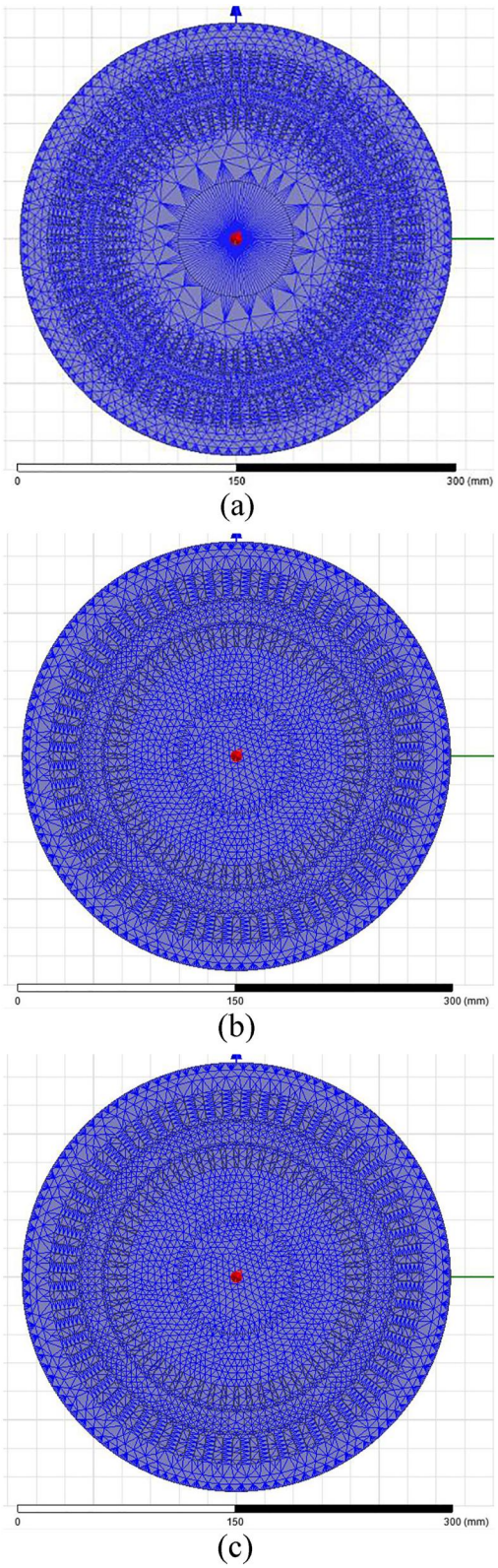

FIGURE 3 Mesh plot of (a) novel dual-stator embedded-pole six-phase permanent magnet synchronous motor (with H-shaped flux barrier), (b) dual stator embedded-pole six-phase permanent magnet synchronous motor (without flux barrier), and (c) single stator single rotor surface-mounted permanent magnet synchronous motor

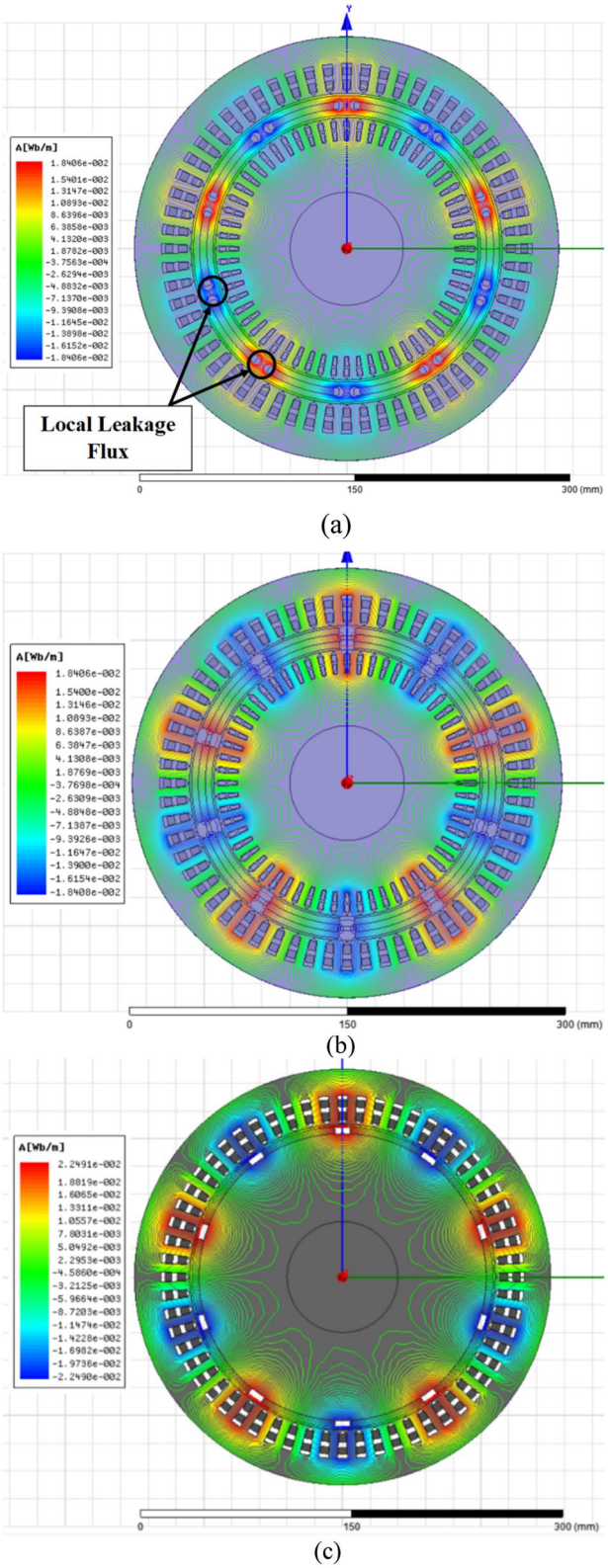

FIGURE 4 Distribution of magnetic field line of (a) dual stator embedded-pole six-phase permanent magnet synchronous motor (without flux barrier) (b) novel dual-stator embedded-pole six-phase permanent magnet synchronous motor (with H-shaped flux barrier), and (c) single stator single rotor surface-mounted permanent magnet synchronous motor

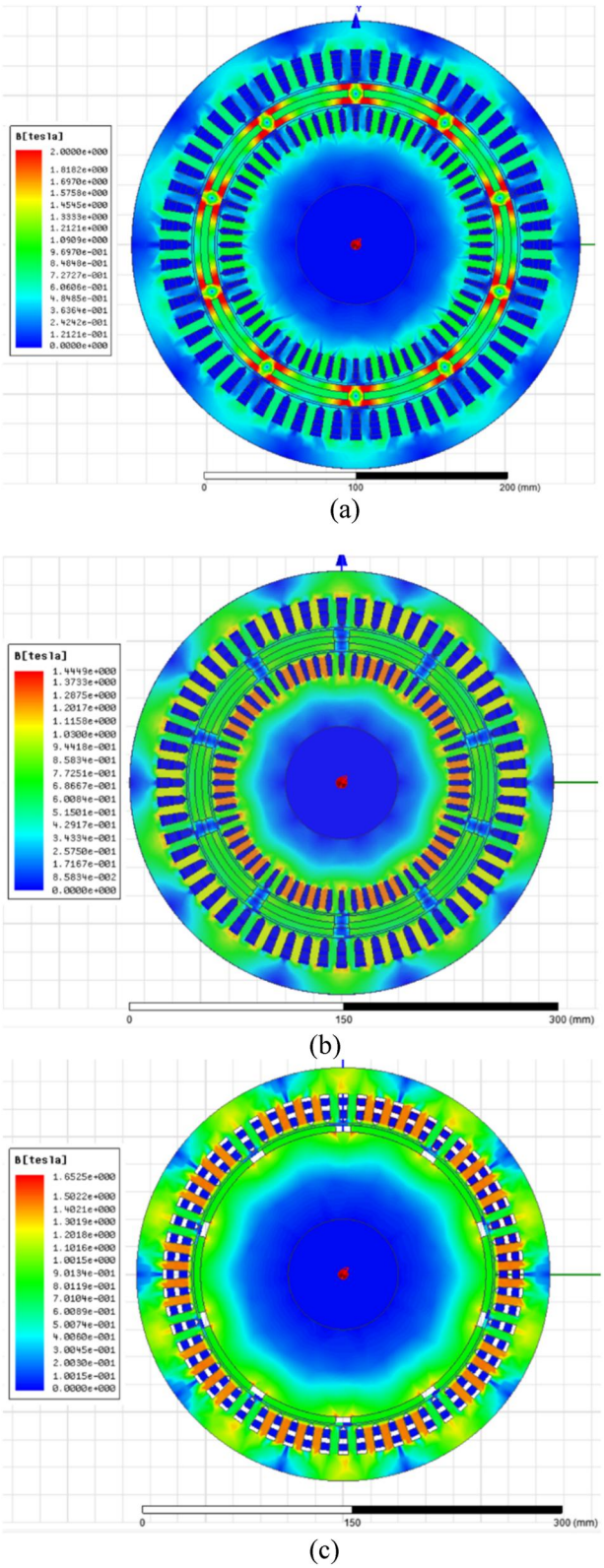

FIGURE 5 Distribution of the magnetic field density of (a) dual stator embedded-pole six-phase permanent magnet synchronous motor (without flux barrier) (b) novel dual-stator embedded-pole six-phase permanent magnet synchronous motor (with an H-shaped flux barrier), and (c) single stator single rotor surface-mounted permanent magnet synchronous motor

suppress this local flux leakage, the authors have introduced the concept of NDSEPSP-PMSM, providing H-Shaped flux barriers between two adjacent magnets in both inward as well as outward rotatory portions, as highlighted in Figure 4b. Here, it has been noted that the flux barrier is not breached by the flux lines, and all the flux passes through the air gap. Thus, this design feature not only eliminates local leakage flux lines but also enhances the overall flux density distribution in the air gap. The flux line distribution of SSSRSM-PMSM is depicted in Figure 4c.

Figure 5a displays the distribution of the magnetic field density of DSEPSP-PMSM (without flux barrier). Using a proper analysis of the figure, the formation of deep red patches in the rotor portion between each adjacent magnet is noticed. The value of flux densities of these portions reaches the saturation level, which shows the drawback of the model. Therefore, to remove this drawback, the authors have introduced the concept of H-shaped flux barriers, as shown in Figure 5b. From the given plot, the flux densities in various regions of NDSEPSP-PMSM are-

a. Outer stator yoke - 0.51501 T
b. Outer stator tooth - 1.05 T
c. Inner stator yoke - 1.030 T
d. Inner stator tooth - 1.2875 T

Also, the magnetic field density in the tooth portion (interior stator) is greater than the other above-calculated values. The magnetic field density of the stator tooth(interior) is also found to be less than that of the maximum allowed saturation level, indicating that the model is precisely built and optimised in nature.

Figure 5c depicts the field density plot of the SSSRSM-PMSM. Both stators as well as the rotor yoke along with the stator tooth have field densities of 1.201 T, 0.6008 T, and 1.301 T. Since these values are below 1.625 T, it is said to be optimally designed.

Figure 6a shows the B-field density in the air gap (interior) for NDSEPSP-PMSM and DSEPSP-PMSM. The values of inner air-gap densities are-

a. NDSEPSP-PMSM - 0.765 T
b. DSEPSP-PMSM - 0.4739 T

Similarly, Figure 6b shows the B-field density in the air gap (outward) for NDSEPSP-PMSM, DSEPSP-PMSM, and SSSRSM-PMSM. The values of the outer air-gap densities are given as follows:

a. NDSEPSP-PMSM - 0.701 T
b. DSEPSP-PMSM - 0.4085 T
c. SSSRSM-PMSM - 0.796 T

The value of the flux density of different topologies is mentioned in Table 4.

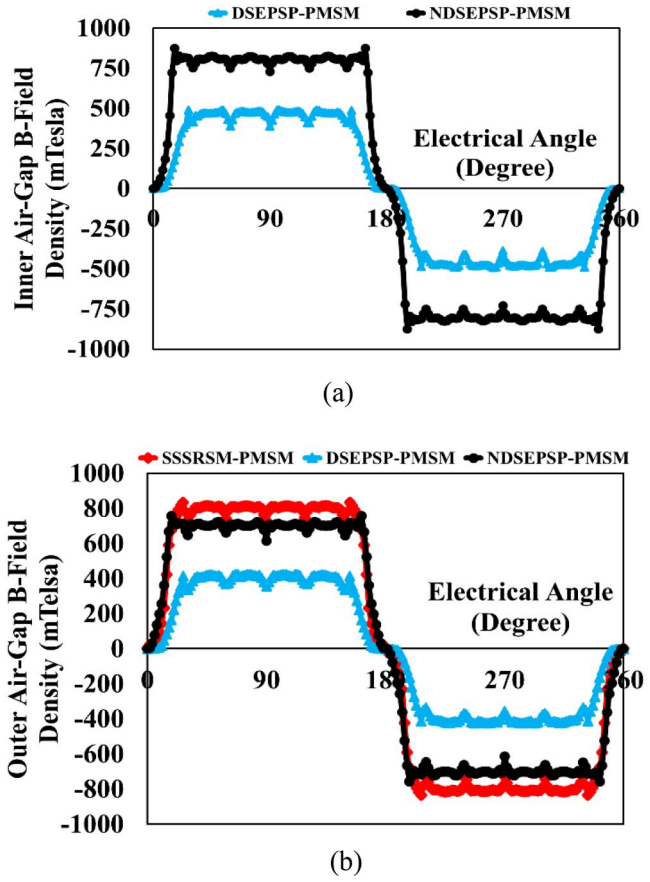

FIGURE 6 Field density of permanent magnet synchronous motors in the (a) Interior air gap and (b) Exterior air gap

4 | RESULTS

Using FEM, the assessment of electromagnetic properties of NDSEPSP-PMSM, DSEPSP-PMSM, and SSSRSM-PMSM have been accomplished. Based on the above investigation, the results for back EMF (BEMF), % THD, the torque developed, % ripple in torque, torque versus current, torque and power versus speed, losses, efficiency, power, and torque density are obtained.

Total BEMF developed in the inner and outer stator is expressed in Equation (1).

$$\mathrm{BEMF}\left(E_{b(i,o)}\right) = N_{\mathrm{ph}(i,o)}\frac{d\phi_{(i,o)}}{\mathrm{dt}} \tag{1}$$

where

$$\phi_{(i,o)} = \int B_g(\theta)_{(i,o)}\,\mathrm{dA} \tag{2}$$

where

$$Bg(\theta)(i,o) = \sum_{m=1,3,5\ldots}^{\infty} Bg(i,o)\sin(m\theta\mathrm{er}) \tag{3}$$

In the above equation, Nph (i,o) represents the number of turns on each phase for both stators, $\Phi(i,o)$represents flux density in both the air gaps, $B_g(\theta)$ (i,o) represents the average flux density of both the air gaps with dA as the air gap area for a small section.

The BEMF of all the six-phases for the outer and inner stator-rotor system are, EbA(i,o), EbB(i,o), EbC(i,o), EbD(i,o), EbE(i,o) and EbF(i,o), which can be expressed by Equation (4).

$$\left.\begin{aligned}
E_{\mathrm{bA}(i,o)}(t) &= \sum_{m=1,3,5\ldots}^{\infty} E_{mE_{m(i,o)}}\sin(m\omega_e t)\\
E_{\mathrm{bB}_{(i,o)}}(t) &= \sum_{m=1,3,5\ldots}^{\infty} E_{m_{(i,o)}}\sin\left(m\omega_e t-\frac{\pi}{3}\right)\\
E_{\mathrm{bC}(i,o)}(t) &= \sum_{m=1,3,5\ldots}^{\infty} E_{m(i,o)}\sin\left(m\omega_e t-\frac{2\pi}{3}\right)\\
E_{\mathrm{bD}(i,o)}(t) &= \sum_{m=1,3,5\ldots}^{\infty} E_{m(i,o)}\sin(m\omega_e t-\pi)\\
E_{\mathrm{bE}_{(i,o)}}(t) &= \sum_{m=1,3,5\ldots}^{\infty} E_{m(i,o)}\sin\left(m\omega_e t-\frac{4\pi}{3}\right)\\
E_{\mathrm{bF}(i,o)}(t) &= \sum_{m=1,3,5\ldots}^{\infty} E_{m_{(i,o)}}\sin\left(m\omega_e t-\frac{5\pi}{3}\right)
\end{aligned}\right\} \tag{4}$$

Where, Em(i,o) depicts the maximum magnitude of BEMF for both the stator portions, m represents the space harmonic indices, and ω_e is the electrical angular speed.

Figure 7a shows the inner stator BEMF of NDSEPSP-PMSM and DSEPSP-PMSM. It has been pointed out that BEMF in the inner stator for the configurations mentioned above is trapezoidal in shape due to the harmonics present in it. The NDSEPSP-PMSM and DSEPSP-PMSM have a magnitude of 110.447 and 68.414 V, respectively. Figure 7b,c show the harmonic (Fast Fourier Transform [FFT]) study of the inner BEMF of NDSEPSP-PMSM and DSEPSP-PMSM, respectively. It can be calculated using Equation (5). The NDSEPSP-PMSM is having a %THD of 30.55%. Similarly, the DSEPSP-PMSM is having a %THD of 20.51%. Except for the multiple of six-order harmonics, the remaining harmonics are obtained in the inner stator BEMF, according to this FFT analysis.

$$\%\ \mathrm{THD} = \frac{\sqrt{\sum_{2}^{\infty} E_n}}{E_1} \times 100 \tag{5}$$

Where En represents the nth harmonic component whereas E_1 represents the fundamental component in BEMF.

Figure 8a shows the BEMF in the outer six-phase ten-pole winding of NDSEPSP-PMSM, DSEPSP-PMSM, and SSSRSM-PMSM. Owing to the presence of harmonics in the outer stator BEMF, it is also trapezoidal in nature. The NDSEPSP-PMSM and DSEPSP-PMSM have BEMF of 221.896 and 129.307 V,

TABLE 4 Comparison of performance parameters

Parameter	NDSEPSP-PMSM	DSEPSP-PMSM	SSSRSM-PMSM
Inner air gap flux density (T)	0.765	0.4739	-
Outer air gap flux density (T)	0.701	0.4085	0.796
Inner stator BEMF (Volts)	110.447	68.414	-
% THD of inner stator BEMF	30.55%	20.51	-
Outer stator BEMF (Volts)	221.896	129.30	261.84
% THD of outer stator BEMF	30.43	25.46	26.69
Torque development on the rotor (Nm)	178.11	101.83	141.336
% Ripple in torque	21.125	29.076	14.406
Cogging torque (Nm)	1.26	0.663	0.98
Power input (kW)	11.185	6.395	8.875
% Efficiency	93.931	89.847	94.161
Torque to weight ratio (Nm/kg)	4.229	2.348	3.166
Losses (Watts)	722.688	702.69	550.363

respectively. On the other hand, the SSSRSM-PMSM has a magnitude of 261.84 V. The FFT study of the outer stator generated voltage of NDSEPSP-PMSM, NDSEPSP-PMSM, and SSSRSM-PMSM are shown in Figure 8b,c,d, respectively. The %THD of the above-mentioned topologies are 30.43%, 25.46%, and 26.69%, respectively. Here also, it is pointed out that in the outer stator BEMF, all harmonics are present other than six-order harmonics. The stator BEMF values and %THD of different topologies are included in Table 4.

The inner and outer stator-rotor motor equation can be expressed by Equation (6).

$$\left[V_{s(\mathrm{i,o})}\right]_{6\mathrm{X}1} = \left[E_{b(\mathrm{i,o})}\right]_{6\mathrm{X}1} + \left[Z_{\mathrm{ph(i,o)}}\right]_{6\mathrm{X}6}\left[I_{\mathrm{ph(i,o)}}\right]_{6\mathrm{X}1} \quad (6)$$

Where [Versus(i.o)]6 × 1, [Eb(i.o)]6 × 1, [Iph(i.o)]6 × 1, and [Zph(i.o)]6 × 6 are having supply volage, BEMF, phase current and phase impedance matrixes for the six-phase inner and outer stator-rotor PMSM system.

The rotor torque can be calculated using Equation (7),

$$\text{Torque} = \frac{P_i - P_L}{w_m} \quad (7)$$

Where Pi is the input power, PL is the total losses, and w_m is the rotor speed of the machine. The %ripple of the torque can be calculated using Equation (8).

$$\%\ \text{Ripple torque} = \frac{T_{\max} - T_{\min}}{T_{\text{avg}}} \times 100 \quad (8)$$

Where $T_{\max}$ is the maximum magnitude, $T_{\min}$ is the minimum magnitude, and T_{avg} is the average torque of the machine.

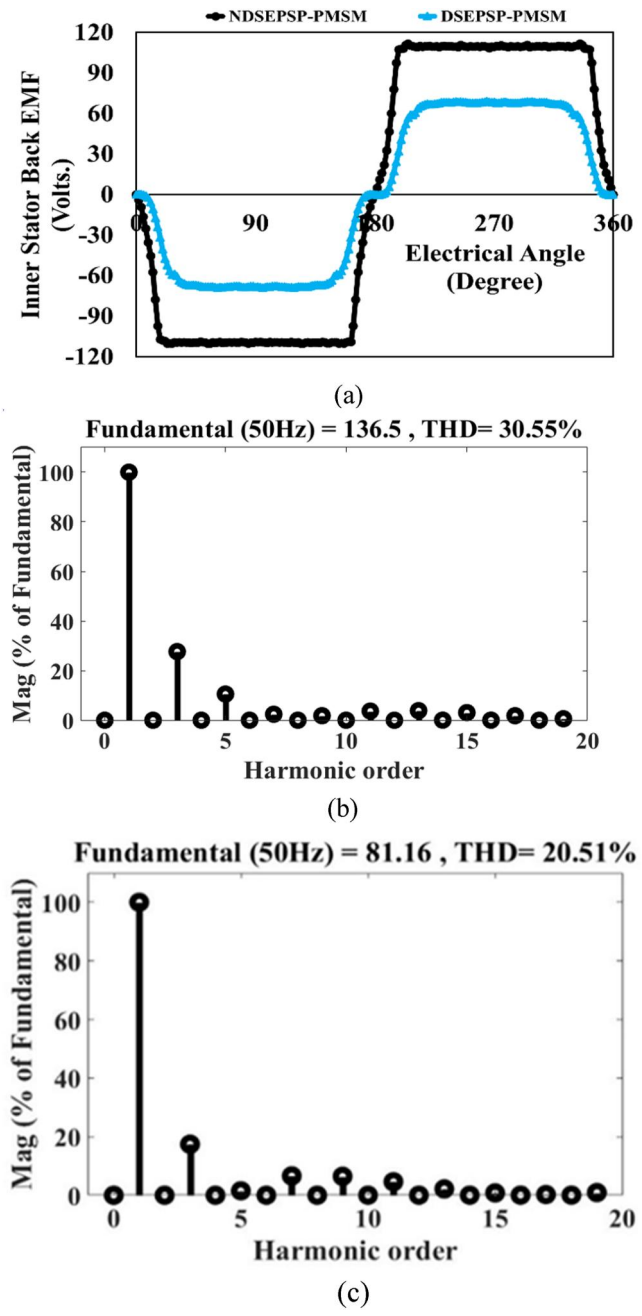

FIGURE 7 Analysis of the inner stator (a) back EMF (BEMF), (b) Fast Fourier Transform (FFT) study of BEMF for a novel dual-stator embedded-pole six-phase permanent magnet synchronous motor, and (c) FFT study of BEMF for a dual stator embedded-pole six-phase permanent magnet synchronous motor

The torque developed on the rotor of different topologies, namely, NDSEPSP-PMSM, DSEPSP-PMSM, and SSSRSM-PMSM is displayed in Figure 9a. The average magnitude of the torque developed in one period of the cycle is as follows:

- NDSEPSP-PMSM - 178.11 Nm
- DSEPSP-PMSM - 101.829 Nm
- SSSRSM-PMSM - 141.336 Nm

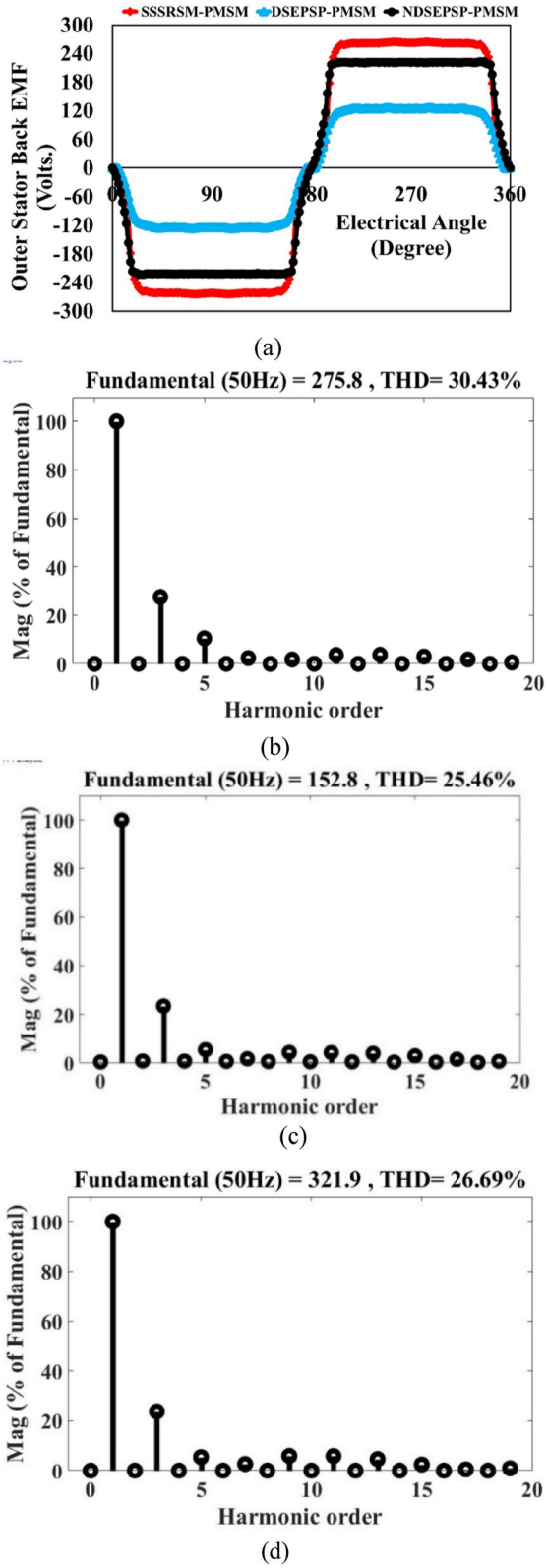

FIGURE 8 Analysis of an exterior Stator (a) back EMF (BEMF), (b) Fast Fourier Transform (FFT) study of BEMF for a novel dual-stator embedded-pole six-phase permanent magnet synchronous motor, (c) FFT study of BEMF for a dual stator embedded-pole six-phase permanent magnet synchronous motor and (d) FFT study of BEMF for a single stator single rotor surface-mounted permanent magnet synchronous motor

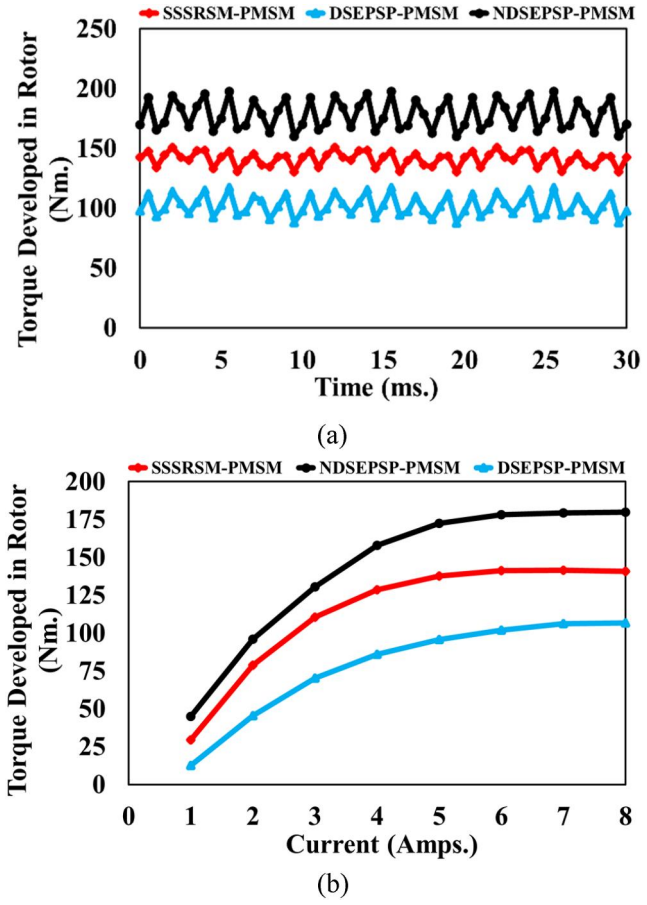

FIGURE 9 Study of (a) Developed Torque and (b) Torque versus current

It is observed from the plot that in NDSEPSP-PMSM, DSEPSP-PMSM, and SSSRSM-PMSM, there are a total of 12 ripples in a single cycle. The %ripple content are observed to be 21.125%, 29.076%, and 14.406%. Table 4 also shows the magnitude of the torque and its %ripple.

Torque versus the current characteristics of NDSEPSP-PMSM, DSEPSP-PMSM, and SSSRSM-PMSM is displayed in Figure 9b. Here, it is observed that for the rated current, the value of the developed torque (rotor) is high for the proposed NDSEPSP-PMSM.

The power versus speed and torque versus speed characteristics of NDSEPSP-PMSM, DSEPSP-PMSM, and SSSRSM-PMSM are displayed in Figure 10a,b,c, respectively. From this plot, the maximum power is observed to be 11.185 kW in NDSEPSP-PMSM, and in DSEPSP-PMSM the maximum power is found to be 6.395 kW. Moreover, the power in SSSRSM-PMSM is found to be 8.876 kW.

The %efficiency of the motor can be computed using Equation (9)

$$\%\ \text{Efficiency} = \frac{P_i - P_L}{P_i} \times 100\% \tag{9}$$

Figure 11, exhibits the efficiency plot for all the above-mentioned topologies. It has been inferred that the efficiency

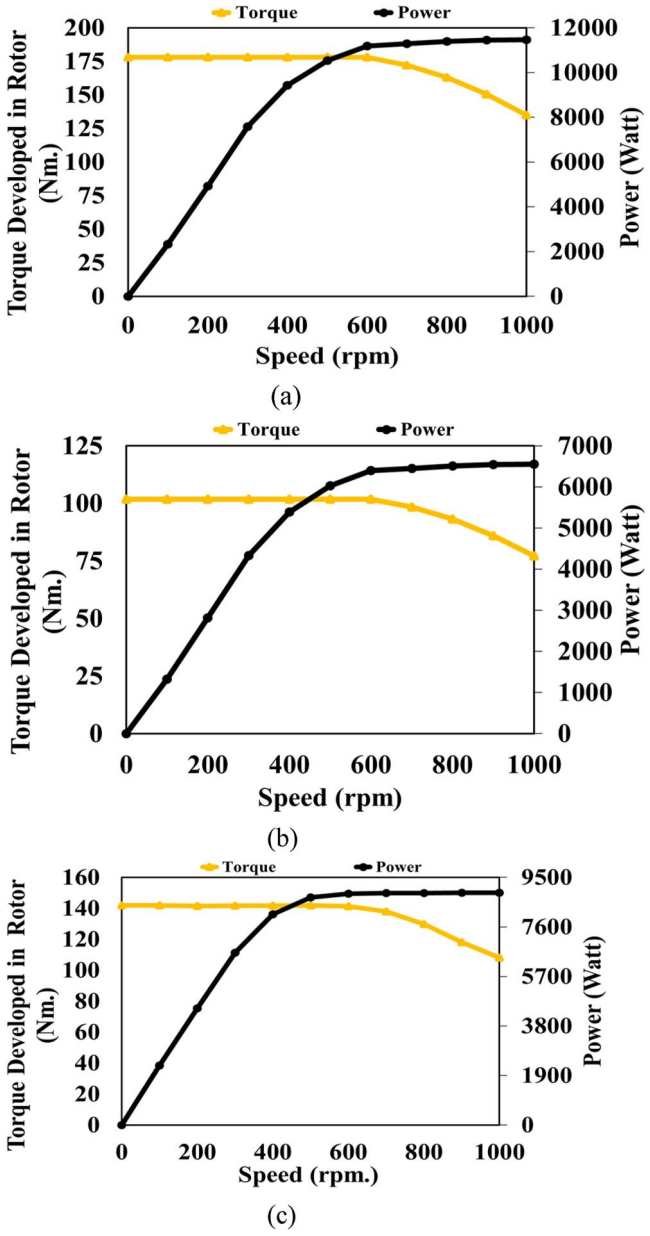

FIGURE 10 Study of (a) Torque and power versus speed characteristics of a novel dual-stator embedded-pole six-phase permanent magnet synchronous motor, (b) Torque and power versus speed characteristics of dual stator embedded-pole six-phase permanent magnet synchronous motor, and (c) Torque and power versus speed characteristics of a single stator single rotor surface-mounted permanent magnet synchronous motor

of NDSEPSP-PMSM, DSEPSP-PMSM, and SSSRSM-PMSM are found to be 93.931%, 89.847%, and 94.161%, respectively. The efficiency of various topologies at a rated current (6 amps) is given in Table 4.

5 | CONCLUSION

This paper has illustrated the characteristics study of an NDSEPSP-PMSM for electric vehicle application. To highlight the performance superiority of the proposed motor, a

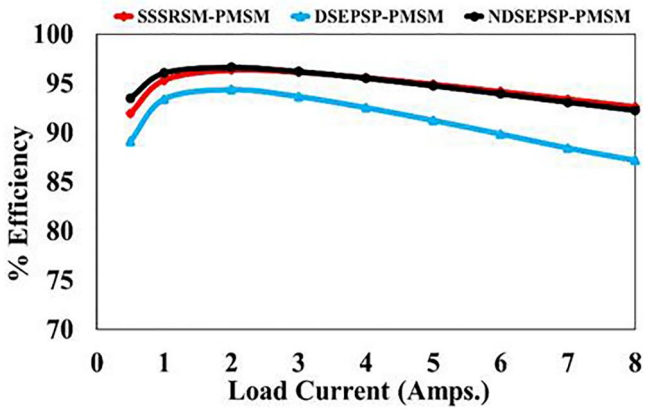

FIGURE 11 Efficiency

comparative study with two different topologies of the motor has been done, namely DSEPSP-PMSM and SSSRSM-PMSM. In addition, for the best-suited design of the proposed motor, a design methodology has also been presented, which provides minimum leakage of fluxes and enhances the overall performance. From the FEM analysis, it is pointed out that the air gap flux density of NDSEPSP-PMSM is superior. Further, at a rated current of 6A, the torque developed in NDSEPSM-PMSM is the highest, that is, 178.11 Nm with a 21.125% ripple content. From the power versus speed and torque versus speed plot, the magnitude of power (of 11.185 kW) and torque is found to be maximum in NDSEPSP-PMSM. The torque densities (torque to weight ratio) for NDSEPSP, DSEPSP, and SSSRSM-PMSM are found to be 4.229 N.m/kg, 2.348 N.m/kg, and 3.166 N.m/kg, respectively. Furthermore, the torque density for the suggested NDSEPSP-PMSM is shown to be the optimum for the same volume of motors. From the comparison of various topologies, the authors have successfully highlighted the advantageous features of the proposed NDSEPSP-PMSM. It is concluded that the proposed motor (NDSEPSP-PMSM) is competent for the EV application due to HTD and good dynamic characteristics.

AUTHOR CONTRIBUTIONS

Raja Ram Kumar: Conceptualisation; Data curation; Formal analysis; Investigation; Methodology; Project administration; Resources; Software; Validation; Visualisation; Writing – original draft. **Priyanka Devi:** Formal analysis; Investigation; Methodology; Project administration; Resources; Software; Validation; Visualisation; Writing – original draft. **Chandan Chetri:** Resources; Software; Supervision; Validation; Visualisation; Writing – original draft; Writing – review & editing. **Ankita Kumari:** Resources; Software; Supervision; Validation; Visualisation; Writing – original draft; Writing – review & editing. **Papu Moni Saikia:** Resources; Software; Supervision; Validation; Visualisation; Writing – original draft; Writing – review & editing. **Ram Khelawan Saket**: Resources; Software; Supervision; Validation; Visualisation; Writing – original draft; Writing – review & editing. **Kundan Kumar:** Resources; Software; Supervision; Validation; Visualisation; Writing –

original draft; Writing – review & editing. **Baseem khan:** Formal analysis; Investigation; Project administration; Resources; Software; Supervision; Validation; Writing – original draft; Writing – review & editing.

ACKNOWLEDGEMENTS

The authors acknowledge the financial support extended by Science and Engineering Research Board (SERB); a statutory body of the Department of Science & Technology (DST), Government of India; New Delhi, India under the sponsored research project sanction order No. EEQ/2021/000177.

CONFLICT OF INTEREST

The authors declare that there is no conflict of interest.

DATA AVAILABILITY STATEMENT

As per journal Policy.

ORCID

Chandan Chetri https://orcid.org/0000-0001-8506-3657
Baseem Khan https://orcid.org/0000-0002-5082-8311

REFERENCES

1. Chatterjee, N.: A time series forecast of geopolitical market concentration (GMC) risk: an analysis of the crude oil diversification portfolio of India. Strat. Anal. 36(1), 145–165 (2012)
2. Zhang, X.B., et al.: Oil import Tariff game for energy Security: the case of China and India. Energy Econ. 72, 255–262 (2018). https://doi.org/10.1016/j.eneco.2018.03.035
3. Wang, J., et al.: Design and performance comparison of novel flux-concentrating IPM machines for power generation system application of extended-range electric vehicle. IEEE Trans. Ind. Electron., 1–10 (2022). https://doi.org/10.1109/TIE.2022.3183341
4. Tu, H., et al.: Extreme fast charging of electric vehicles: a Technology overview. IEEE Trans. on Transp. Electrific. 5(4), 861–878 (2019). https://doi.org/10.1109/tte.2019.2958709
5. Khurana, A., Ravi Kumar, V.V., Sidhpuria, M.: A study on the adoption of electric vehicles in India: the mediating role of attitude. Vision. 24(1), 23–34 (2020). https://doi.org/10.1177/0972262919875548
6. Bilatiu, C., et al.: Identification and evaluation of electric and hybrid vehicles propulsion system. In: Electric Vehicles Int. Conf. (EVIC), pp. 1–5 (2019)
7. Zakaria, H., et al.: Recent advancements and developments for electric vehicle Technology. In: Int. Conf. of Comput. Sci. and Renewable Energies (ICCSRE), pp. 1–6 (2019)
8. Wu, J., et al.: Robust optimization of a rare-earth-reduced high-torque-density PM motors for electric vehicles based on parameter sensitivity region. In: IEEE Transactions on Vehicular Technology, pp. 1–11 (2022). https://doi.org/10.1109/TVT.2022.3183503
9. Hassanin, M., et al.: Operation of BLDC motor to drive the electric vehicle. In: 20th International Middle East Power Systems Conference (MEPCON), pp. 500–503. Cairo (2018)
10. Karki, A., et al.: Status of pure electric vehicle power train Technology and future prospects. Appl. Syst. Innov. 3(35), 35 (2020). https://doi.org/10.3390/asi3030035
11. Lee, T., et al.: Motor design and characteristics comparison of outer-rotor-type BLDC motor and BLAC motor based on numerical analysis. IEEE Trans. Appl. Supercond. 26(4), 1–6 (2016). Art no. 5205506. https://doi.org/10.1109/tasc.2016.2548079
12. Son, J.-C., et al.: Performance enhancement of the IPMSM for HEV applications using grain-oriented electrical steel and design optimization. IEEE Access. 10, 46599–46607 (2022). https://doi.org/10.1109/access.2022.3170896
13. Wang, H., Leng, J.: Summary on development of permanent magnet synchronous motor. In: Chinese Control and Decision Conf. (CCDC), pp. 689–693. Shenyang, China (2018)
14. Kothari, D.P., Nagrath, I.J., Saket, R.K.: Modern Power System Analysis, 5th ed, pp. 1–850. McGraw Hill publication, New Delhi (2022). Publication date: June 10, 2022
15. Shentu, L., et al.: Design and analysis of a direct-drive permanent magnet vernier motor for electric drilling applications. In: 21st Int. Conf. on Elect Mach. and Syst. (ICEMS), pp. 81–86. Jeju, Korea (South) (2018)
16. Jeong, C., Park, J., Bianchi, N.: Alternatives to replace rare-earth permanent magnet motors in direct drive applications. In: Int. Symp. on Power Electron., Elect. Drives; Automat. and Motion (SPEEDAM), pp. 276–281. Sorrento, Italy (2020)
17. Fan, Y., et al.: Design and analysis of a new interior permanent magnet motor for EVs. In: 8th Int. Power Electron. and Motion Control Conf. (IPEMC-ECCE Asia), pp. 1357–1361. Hefei, China (2016)
18. Lyutarevich, A.G., Dolinger, S.Y., Plankov, A.A.: Development of permanent magnet motor calculation technique. In: 2nd Int. Conf. on Ind. Eng., Appl. and Manuf. (ICIEAM), pp. 1–5. Chelyabinsk (2016)
19. Kumar, R.R., et al.: Modeling of airgap fluxes and performance analysis of five-phase permanent magnet synchronous generator for wind-power application. IEEE Access. 8, 195472–195486 (2020). https://doi.org/10.1109/access.2020.3034268
20. Bhatt, P., Mehar, H., Sahajwani, M.: Electrical motors for electric vehicle – a comparative study. In: Proceed. of Recent Advances in Interdisciplinary Trends in Eng. & Appl. (RAITEA). SSRN-ELSEVEIR (2019)
21. Trajkovski, D., Cvetkovski, G.: Performance analysis of different rotor topologies in permanent magnet motor. In: EUROCON 2017 -17th Int. Conf. on Smart Technol. pp. 411–416. Ohrid, Macedonia (2017)
22. Dinh, B.M., Linh, D.H.: Electromagnetic and thermal calculation of surface mounted permanent magnet motor using finite element method. In: Int. Conf. on Sustain. Energy Technol. (ICSET). pp. 355–358. Hanoi (2016)
23. Seol, H.-S., et al.: Design of 3-times magnetizer and rotor of spoke-type PMSM considering post-assembly magnetization. IEEE Trans. Magn. 53(11), 1–5 (2017). Art no. 8208005. https://doi.org/10.1109/tmag.2017.2707593
24. Thangaraj, B., Arumugam, D., Somasundaram, G.: FEA analysis of S-PMSG for aircraft application. Int. J. Eng. Technol. 7, 89–93 (2018)
25. Woo, D., Jeong, B.H.: Irreversible demagnetization of permanent magnet in a surface-mounted permanent magnet motor with overhang structure. IEEE Trans. Magn. 52(4), 1–6 (2016). https://doi.org/10.1109/tmag.2015.2476782
26. Dong, J., et al.: Comparative study of surface-mounted and interior permanent-magnet motors for high-speed applications. IEEE Trans. Appl. Supercond. 26(4), 1–4 (2016). https://doi.org/10.1109/tasc.2016.2514342
27. Ocak, O., Onsal, M., Aydin, M.: Development of a 7.5kW high speed interior permanent magnet synchronous spindle motor for CNC milling machine. In: XIII Int. Conf. on Elect. Mach. (ICEM). Alexandroupoli, Greece (2018)
28. Xie, S., et al.: A consequent-Pole magnetic-geared machine with axially embedded permanent magnets for hybrid electric vehicle. IEEE Access. 9, 14905–14917 (2021). https://doi.org/10.1109/access.2021.3052914
29. Petrov, I., et al.: Unequal teeth widths for torque ripple reduction in permanent magnet synchronous machines with fractional-slot non-overlapping windings. IEEE Trans. Magn. 51(2), 1–9 (2015). Art no. 8100309. https://doi.org/10.1109/tmag.2014.2355178
30. Farmahini Farahani, E., Jalali Kondelaji, M.A., Mirsalim, M.: A new exterior-rotor multiple teeth switched reluctance motor with embedded permanent magnets for torque enhancement. IEEE Trans. Magn. 56(2), 1–5 (2020). Art no. 8100405. https://doi.org/10.1109/tmag.2019.2955884
31. Huynh, T.A., Hsieh, M.: Irreversible demagnetization analysis for multilayer magnets of permanent magnet-assisted synchronous reluctance machines considering current phase angle. IEEE Trans. Magn. 55(7), 1–9 (2019). Art no. 8106609. https://doi.org/10.1109/tmag.2019.2911867

32. Yang, S., et al.: Design of double stator permanent magnet synchronous motor with low-speed large torque. In: Student Conf. on Elect. Mach. and Syst. pp. 1–6. Huzhou, China (2018)
33. Asgari, S., Mirsalim, M.: A novel dual-stator radial-flux machine with diametrically magnetized cylindrical permanent magnets. IEEE Trans. Ind. Electron. 66(5), 3605–3614 (2019). https://doi.org/10.1109/tie.2018.2856211
34. Kumar, R.R., et al.: Thermal analysis of five-phase PMSG for small-scale wind power application. Int. J. Mech. Prod. Eng. Res. Dev. 8(6), 667–680 (2018). https://doi.org/10.24247/ijmperddec201869
35. Kumar, R.R., et al.: Design and analysis of dual stator non-magnetic rotor six-phase permanent magnet synchronous generator for marine power application. In: 2020 IEEE Int. Conf. on Comput., Power and Communication Technol. (GUCON), pp. 582–586 (2020)
36. Xie, Y., Ning, Z., Ma, Z.: Comparative study on variable flux memory machines with different arrangements of permanent magnets. IEEE Access. 8, 164304–164312 (2020). https://doi.org/10.1109/access.2020.3022595
37. Huynh, T.A., Hsieh, M.: Performance analysis of permanent magnet motors for electric-vehicles (EV) traction considering driving cycles. Energies. 11(6), 1–24 (2018). https://doi.org/10.3390/en11061385
38. Kim, K., Lee, B.: Comparative study of concentrated flux synchronous motor and multi-layer IPMSM for traction drives using non-rare earth permanent magnet. IET Electr. Power Appl. 14(9), 1686–1691 (2020). https://doi.org/10.1049/iet-epa.2020.0048
39. Dong, J., et al.: Comparative study of surface-mounted and interior permanent magnet motors for high-speed applications. IEEE Trans. Appl. Supercond. 26(4), 1–4 (2016). Art no. 5200304. https://doi.org/10.1109/tasc.2016.2514342
40. Liu, X., et al.: Comparison and design optimization of a five-phase flux-switching PM machine for in-wheel traction applications. IEEE Trans. Energy Convers. 34(4), 1805–1817 (2019). https://doi.org/10.1109/tec.2019.2921921
41. Kumar, R.R., et al.: Design and characteristic investigation of novel dual-stator V-shaped magnetic Pole six-phase permanent magnet synchronous generator for wind power application. Elec. Power Compon. Syst. 48(14-15), 1537–1550 (2020). https://doi.org/10.1080/15325008.2020.1854388
42. Jung, S.-W., et al.: Comparative design study of HTS synchronous motor with inner and outer rotor type based on multi-objective optimization. IEEE Trans. Appl. Supercond. 32(6), 1–5 (2022). Art no. 5202305. https://doi.org/10.1109/tasc.2022.3168619
43. Qi, J., et al.: Effect of Pole shaping on torque characteristics of consequent Pole PM machines. IEEE Trans. Ind. Appl. 58(3), 3511–3521 (2022). https://doi.org/10.1109/tia.2022.3156904

How to cite this article: Kumar, R.R., et al.: Performance analysis of dual stator six-phase embedded-pole permanent magnet synchronous motor for electric vehicle application. IET Electr. Syst. Transp. e12063 (2023). https://doi.org/10.1049/els2.12063